ELSEVIER

Biochimica et Biophysica Acta 1185 (1994) 160–166

BBA Biochimica et Biophysica Acta

Blue form of bacteriorhodopsin and its order–disorder transition during dehydration

Soichi Wakatsuki [a,1], Yoshiaki Kimura [b,2], Walther Stoeckenius [b], Nanna Gillis [c], David Eliezer [d], Keith O. Hodgson [a,*], Sebastian Doniach [c]

[a] *Department of Chemistry and Stanford Synchrotron Radiation Laboratory, Stanford University, Stanford, CA 94305, USA;* [b] *Cardiovascular Research Institute, University of California, San Francisco, CA 94143, USA;* [c] *Department of Applied Physics, Stanford University, Stanford, CA 94305, USA;* [d] *Department of Physics, Stanford University, Stanford, CA 94305, USA*

(Received 15 July 1993; revised manuscript received 4 November 1993)

Abstract

Freshly-prepared blue membranes from *Halobacterium halobium*, previously reported to be disordered, are shown to have a distinct crystal lattice structure, slightly different from the native form. The lattice of the blue form is disrupted irreversibly when dehydrated. The disorder process was observed using time-resolved small-angle X-ray diffraction and analyzed by radial autocorrelation functions. The diffraction peaks of the in-plane lattice first sharpen and increase due to improved membrane orientation, then the trimer lattice becomes disordered and the unit cell dimension decreases by 1.8 Å. In contrast, dehydration of purple membranes does not disorder the lattice, and the unit cell dimension shrinks by only 1.0 Å. Comparisons of radial autocorrelation functions for the blue membrane during drying show drastic loss of inter-trimer, long-range correlation while the intra-trimer, short-range correlations remain more or less unchanged. This suggests that the deionized protein trimers can maintain their overall structure during the dehydration, even though the lattice dimension decreases appreciably and the two-dimensional crystallinity is disrupted.

Key words: Time-resolved small-angle X-ray diffraction; Blue membrane; Deionized purple membrane; Order–disorder transition; Radial autocorrelation function; Dehydration

1. Introduction

The purple membrane (PM) is a natural two-dimensional (2D) crystal from cell membranes of *Halobacterium halobium* [1]. Purple membrane consists of highly acidic lipids and the membrane protein, bacteriorhodopsin (bR). This retinylidene protein functions as a light-driven proton pump [1]. The structure of PM has been studied extensively by electron microscopy (EM) [2–4], X-ray [5–7] and neutron diffraction [8–10]. Acidification shifts the 568 nm absorption maximum of bR to 605 nm near pH 3.0, at low ionic strength, producing the blue membrane [11–13]. This reversible transition is also obtained by removal of residual cations with an ion exchange resin [14], which results in a surface pH below 2 [15,16]. The blue form of bR does not function as a proton pump [12,13]. It apparently contains several coexisting chromophore conformers: 13-*cis* and 13-*trans* retinals, syn-C=N- and anti-C=N-Schiff base bonds [17]. Modification of ASP85, ASP212 and ARG82, TYR185 affect the purple-to-blue transition [18,19] but the acid-induced absorbance shift is caused mainly by weakening of the counterion due to protonation of ASP85 [20] and the blue form of bR may be related to the O-intermediate of the photocycle [21,22]. Therefore, the determination of any structural changes that accompany the purple-to-blue transition can give insights into the changes in ionic environment around the Schiff base which deactivate the pump. However, contradictory descriptions of the structure of blue membranes have appeared, claiming a well-pre-

* Corresponding author. Fax: +1 (415) 7234817.
Present addresses: [1] Laboratory of Molecular Biophysics, Oxford, UK; [2] Protein Engineering Research Institute, Osaka, Japan.
Abbreviations: PM, purple membrane; EM, electron microscopy; bR, bacteriorhodopsin; SAXD, small-angle X-ray diffraction.

SSDI 0005-2728(93)E0208-8

served lattice [14] or a disordered lattice [13,23]. It has been suggested that salt bridges near the membrane surface which stabilize the native structure are broken because of the low surface pH of the blue membranes, and therefore the 2D lattice loses long-range order [15,16,23], thus preventing structure determination by X-ray diffraction.

Low-dose EM, a key technique for elucidation of crystalline membrane protein structures, cannot be easily applied to the blue membranes, because cation contamination from grids and dehydration are difficult to avoid and absorption spectroscopy to verify the maintenance of the blue state is practically impossible. In contrast, the small-angle X-ray diffraction (SAXD) technique can be used to study structures of membrane proteins under conditions closer to the physiological environment (humidity, pH, ionic strength, etc.). SAXD is particularly informative when high intensity synchrotron X-ray sources are used for studying time-dependent structural changes. We have observed that one can obtain an X-ray diffraction pattern of the 2D lattice from freshly-prepared fully-hydrated blue membrane, comparable in quality to that from PM. However, the diffraction peaks of blue membrane disappear irreversibly during a few hours of dehydration at ambient relative humidity. In this report, we discuss the effects of hydration on screening of protein–protein interactions and the order–disorder transition of the 2D crystal during dehydration of blue membrane as deduced from time-resolved radial autocorrelation functions.

2. Materials and methods

Sample preparation

Two strains of *Halobacterium halobium* were used: naturally growing JW3 and retinal deficient JW5. For the latter, retinal was added to JW5 culture media at certain times according to the method of Seiff et al. [24]. All other conditions for growing bacteria and purifying PM were the same as those described in [25]. Purple membranes were washed carefully by centrifugation at $30\,000 \times g$. The blue forms have been obtained by deionization instead of acidification since the latter method tends to have a problem of aggregation. The deionization process was according to the method described earlier [14]. Pellet samples of purple or blue membrane were made by ultracentrifugation at $300\,000 \times g$ for about 10 h into a cell with mylar windows on both sides. The size of such pellets is typically $1 \times 1 \times 1$ mm. After centrifugation, the cells were sealed with Corning vacuum grease. To observe dehydration of the membranes, the vacuum grease seal was removed from the sample cells immediately before X-ray exposure. The mosaic spread of the pellets was 10 to 15 degrees initially (half-width-half-height), but is suspected to have improved during the early stages of dehydration, as evidenced by the increased intensity of the in-plane reflections (see below).

To verify the integrity of the blue samples, the dehydrated pellets were recovered after X-ray exposure and resuspended into water in order to measure their optical spectra in suspension. In all cases, the optical spectra of the blue forms before and after X-ray exposure had the same absorption maxima (600 to 603 nm), and no shoulder at 568 nm. It is highly unlikely that the blue form becomes purple in the pellet form and then returns to blue when resuspended into water. In fact, we measured an absorption spectrum of a dried film of deionized blue membrane and found the same λ_{max} as in suspension. Therefore we conclude that the blue membrane pellets prepared as above were indeed the deionized form of purple membrane.

X-ray diffraction

A quadrant position sensitive detector developed by A. Gabriel of EMBL in Grenoble [26] was utilized with the SSRL Small Angle X-ray Scattering/Diffraction camera [27–30] with additional electronics modules and minimal software changes. The 60° fan-shape active area of the quadrant detector is suitable for acquisition of diffraction patterns from moderately oriented membranes such as pelleted PM. The entire system with the quadrant detector, VAXstation II, CAMAC modules, and NIM modules was sent to the National Synchrotron Light Source (NSLS), Brookhaven National Laboratory and rebuilt on beamline X14A [31] to acquire the static and time-resolved X-ray diffraction data. The storage ring at NSLS was operated at 2.5 GeV and typical current was 100 to 200 mA. The X-ray beam of the beamline 14A was focused and monochromatized by a constant offset monochrometer. Additional data were collected using the same system on beamlines 4–2 (8-pole wiggler) and 2–1 (bending magnet) at SSRL operating at the storage ring energy of 3.0 GeV and current of 30 to 100 mA. The X-ray wavelength was 1.65 Å in both cases. Each data set consists of 20 cycles of 10 min exposure. The temperature of the samples during X-ray exposure was kept between 5 and 10°C by circulating cooled water using a digitally-controlled circulation bath, VWR 1145 (VWR Scientific, San Francisco, CA).

The autocorrelation function of a 2D lattice system is defined by

$$A(\mathbf{u}) = \frac{1}{S}\int_S \sigma(\mathbf{r})\sigma(\mathbf{r}-\mathbf{u})\,d\mathbf{r} = \int_{S^*} I(\mathbf{S})\,\exp(2\pi \mathbf{S}r)\,d\mathbf{S}$$

where S is the area for integration, S^* that in the reciprocal space, $\sigma(\mathbf{r})$ electron density profile, $\mathbf{r}$ and $\mathbf{u}$ vectors in real space, $I(\mathbf{S})$ scattering intensity, and $\mathbf{S}$

scattering vector. Since our oriented membranes have random rotation of the membrane patches around their c-axis, only the cylindrical average of the autocorrelation function is significant. Thus, a radial autocorrelation function is a Bessel-Fourier transformation of X-ray diffraction profiles,

$$A_o(u) = \int_{S_{min}}^{S_{max}} I(S) J_0(2\pi S u) 2\pi S \, dS \quad (1)$$

where $J_0(x)$ is a Bessel function of zero order, $I(S)$ is a background-subtracted diffraction intensity profile, and S the modulus of the scattering vector.

3. Results and discussion

Comparison of diffraction patterns from blue and purple membranes

We first compared X-ray diffraction patterns of purple and blue forms using two different PMs: one from strain JW3 and the other from the retinal-deficient mutant JW5 reconstituted with retinal, both of which gave similar results. Fig. 1 shows the differences between purple and blue forms before and after drying. The diffraction pattern of the blue membrane (Fig. 1C) clearly shows in-plane diffraction peaks characteristic of an ordered lattice structure similar to PM. However, after dehydration, the diffraction peaks of blue membranes have significantly broadened (Fig. 1D), suggesting disordering of the lattice upon drying. The dried blue membranes also show a sharp peak at 50.0 Å. This peak cannot be a (1,0) reflection since that would appear at 55 Å. Neither can this reflection arise from a lipid phase transition which would have a characteristic spacing with a much shorter range.

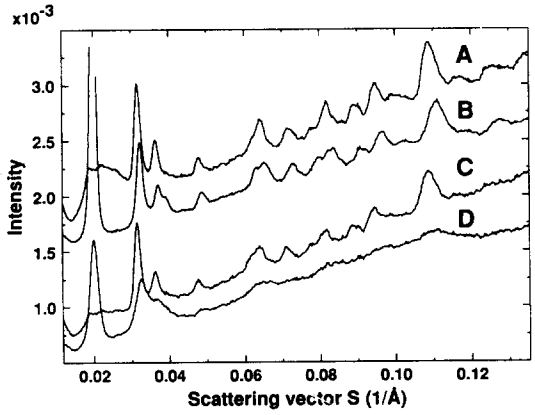

Fig. 1. X-ray diffraction patterns of the purple and blue membranes from JW5 mutant of bR before and after dehydration for 4 h. See text for details of the experimental conditions and data acquisition procedures. (A) Purple membrane before dehydration; (B) purple membrane after dehydration; (C) blue membrane before dehydration; (D) blue membrane after dehydration.

Therefore we conclude that it is an inter-membrane Bragg reflection peak that arises from lamellar stacking of membranes when they are dried. The 60°-fan-shape active area of the quadrant detector enabled the simultaneous observation of in-plane and meridional diffraction. Henderson reported that the spacing of the inter-membrane diffraction peak depends on pH [6]. From Table 1 of his report, we obtained a linear regression, $D = 0.647$ pH + 46.40 (Å) with $R = 0.807$, according to which the inter-membrane spacing of 50.0 Å corresponds to pH about 5.5. As a control experiment, the diffraction patterns of PM were also compared before (Fig. 1A) and after drying (Fig. 1B). In this case, the in-plane diffraction peaks did not disappear, but the 50.0 Å inter-membrane Bragg peak appeared during drying. In addition, two controls were performed to check for possible effects from radiation damage. Blue membrane samples were allowed to dehydrate both after a short exposure to radiation to verify that they did initially diffract, and without any radiation exposure whatsoever. In both cases, measurements from the final dehydrated samples yielded data identical to those obtained at the end of the continuous exposure experiments. This indicates strongly that it is the dehydration of the samples and not radiation damage which is responsible for the observed process.

Time-resolved X-ray diffraction of the order–disorder transition of blue membrane during dehydration

In order to examine the disordering process of the blue form during dehydration, the time course of changes for the in-plane X-ray diffraction patterns of blue membranes was recorded during 4 h of drying at room temperature (Fig. 2A). The in-plane diffraction peaks whose S range is between 0.03 and 0.12 Å^{-1} (where $S = 2\sin\theta/\lambda$, 2θ is the scattering angle and λ is the X-ray wavelength) were lost after about 150 min and an inter-membrane Bragg peak at 50.0 Å appeared at about the same time. The in-plane diffraction peaks grow during the first 100 min but decay and broaden rather rapidly thereafter (Fig. 2B). During the latter half of the dehydration, the peaks become weaker and broader until most of the peaks merge into smooth diffuse scattering peaks. The diffraction pattern after the dehydration is similar to that of PM heated above 80°C [32], but still shows some residual 2D diffraction peaks. We argue below that the broadening is caused by inter-trimer disorder. The order–disorder is irreversible in that any of our attempts to rehydrate partially-dehydrated blue membranes did not result in recovery of the in-plane diffraction.

Radial autocorrelation function

Use of the time-resolved X-ray diffraction patterns to calculate a series of electron density maps during dehydration is not justifiable because of the lack of

appropriate phase information. The patterns change drastically and therefore the broadened peaks of the dehydrated membranes may not have the same phases as those in the hydrated state. However, calculation of radial autocorrelation functions [33] does not require phase information, and does not assume any models except for a random in-plane rotation of the membrane patches. Yet the resulting autocorrelation functions can elucidate many features of structural changes in real space: degree of crystallinity, size of the unit cell, change in correlation at a specific distance, etc. Most of these are not readily seen in diffraction patterns.

We have calculated radial autocorrelation functions for the background-subtracted diffraction patterns in Fig. 2A using the range of S between 0.029 $Å^{-1}$ and 0.125 $Å^{-1}$, excluding the 50.0 Å inter-membrane Bragg

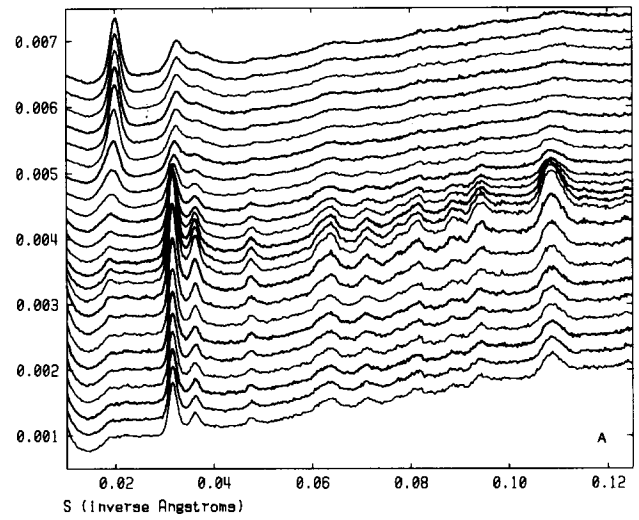

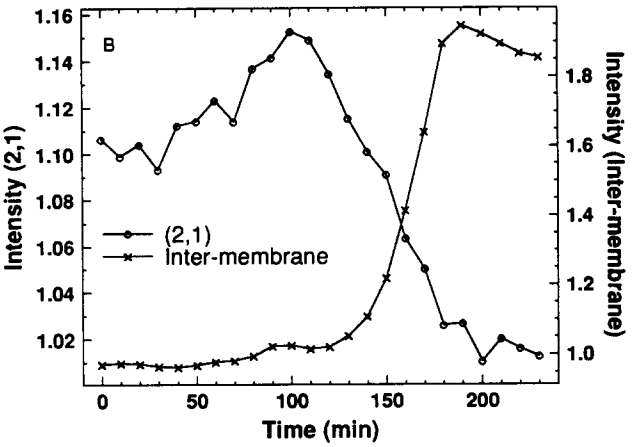

Fig. 2. (A) Time-resolved X-ray diffraction patterns of the blue membrane (JW5) during dehydration. Exposure time of each pattern was 10 min and the entire data set was recorded in 4 h. Calibrated data before background subtraction are plotted with offset; the bottom profile is the first 10 min. (B) Changes in peak heights of an in-plane diffraction peak (2,1) and of the inter-membrane Bragg peak at 50.0 Å during the 4-h drying experiment.

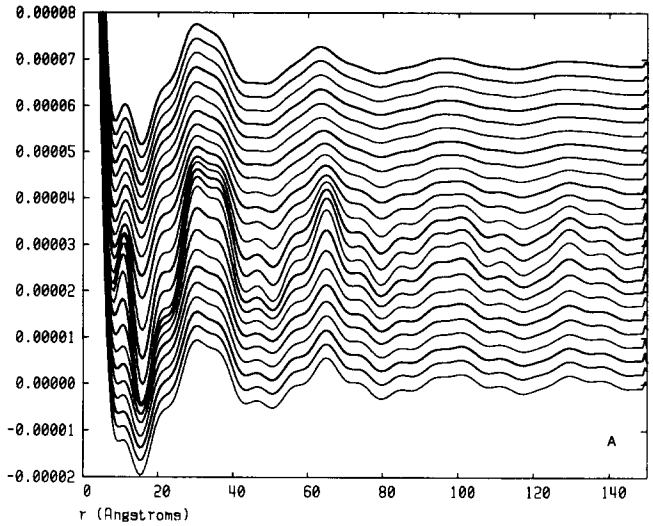

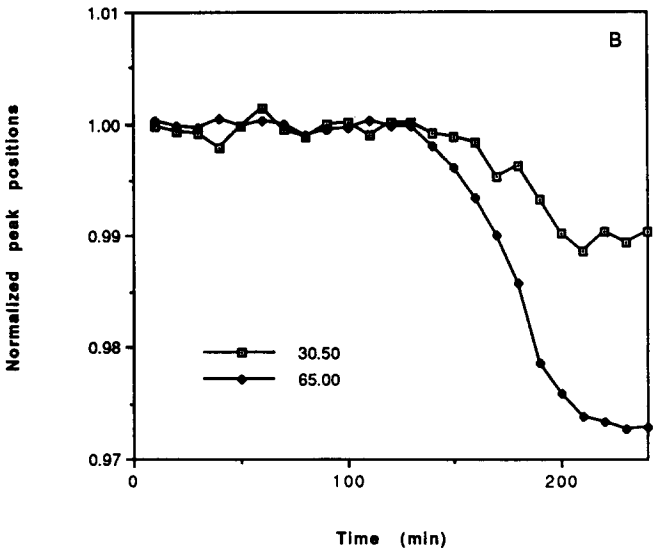

Fig. 3. (A) Time-resolved radial autocorrelation functions during dehydration calculated from data in Fig. 2A in the S range between 0.029 $Å^{-1}$ and 0.125 $Å^{-1}$ using Eq. (1). Here $I(S)$ is an X-ray diffraction intensity profile corrected for the detector active area and background-subtracted. The profiles are plotted with offset, the bottom being the first. Note that the peaks at 65.0 Å and 130.0 Å, corresponding to D and 2D respectively, shift toward shorter range order during the last 2 h. (B) Time changes of normalized peak positions at 30.5 Å and 65.0 Å of the autocorrelation functions. The peak at 30.5 Å is related to both intra- and inter-monomer helix-helix correlation whereas the one at 65.0 Å arises from the unit cell repeat. Positions are normalized by those at the beginning of dehydration. Contraction of 35 Å peak is only 0.3 Å as opposed to 1.8 Å in the case of the 65.0 Å peak. Note that the peak positions remain constant during the first 140 min, while the diffraction peak grows for the first 100 min and starts decreasing rapidly thereafter.

peak since only the in-plane structure is of interest here. As expected from the time change in the X-ray diffraction patterns (Fig. 2A), autocorrelation peaks become sharper during the first 100 min but then become broader and lower (Fig. 3A). Peak broadening

is best described quantitatively by a second derivative of the autocorrelation function. For instance, when blue membranes are still hydrated, second derivatives at 30.5 Å and 65.0 Å yield $1.0 \cdot 10^{-5}$ Å^{-2} and $7.1 \cdot 10^{-5}$ Å^{-2} respectively which change after dehydration to $0.9 \cdot 10^{-5}$ Å^{-2} and $3.0 \cdot 10^{-5}$ Å^{-2}, demonstrating the drastic broadening of the peak at 65.0 Å but a much smaller change in the intra-trimer peak at 30.5 Å. In contrast, dried PMs do not show any appreciable broadening.

The position of the peak at 65.0 Å, which corresponds to the unit cell dimension *, remains constant during the first 100 min, then it starts to shift until it reaches 63.2 Å (Fig. 3B). The decrease results from a contraction of the 2D lattice during the latter half of the dehydration process. Purple membranes also show a decrease in lattice dimension * by 1.0 Å from 64.6 Å to 63.6 Å (from A to B of Fig. 4). A similar decrease of the 2D lattice was observed earlier [5]. Interestingly, the peaks between 20 and 40 Å in the diffraction patterns of blue membranes show much smaller changes in their positions, for example, from 30.5 Å to 30.2 Å (Fig. 3B). If the short-range peaks would arise entirely from correlations between helices in different trimers, shifts of their positions should be proportional to that of the peak at 65.0 Å; the position of the 30.5 Å peak should be shifted by 0.84 Å. Instead it shrank only by 0.3 Å, 36% of the expected change (Fig. 3B).

In order to correlate these shifts of the peaks in the autocorrelation functions with possible movements of protein and lipids, we estimated contributions of intra-trimer and inter-trimer correlations in autocorrelation functions. We define a trimer region simply as a hexagon with side $D/\sqrt{3}$ centered at the origin;

$$S_{\text{hex}}: \begin{cases} -\dfrac{D}{2} \le x \le \dfrac{D}{2} \\ -\dfrac{D}{2} \le \frac{1}{2}x + \dfrac{\sqrt{3}}{2}y \le \dfrac{D}{2} \\ -\dfrac{D}{2} \le \frac{1}{2}x - \dfrac{\sqrt{3}}{2}y \le \dfrac{D}{2} \end{cases}$$

where D is unit-cell dimension. Contributions of intra- and inter-trimer correlations are estimated numerically using the following equation:

$$A_{0,\text{Intra}}(\mathbf{u}) = \int_{S_{\text{Hex}}} \rho(\mathbf{r}) w(\mathbf{r}-\mathbf{u}) \rho(\mathbf{r}-\mathbf{u})\, d\mathbf{r} \quad (2)$$

$$A_{0,\text{Inter}}(\mathbf{u}) = \int_{S_{\text{Hex}}} \rho(\mathbf{r})(1 - w(\mathbf{r}-\mathbf{u}))\rho(\mathbf{r}-\mathbf{u})\, d\mathbf{r} \quad (3)$$

where $\rho(\mathbf{r})$ is electron density at position $\mathbf{r}$, $w(\mathbf{x})$ is a weight function, and

$$\begin{cases} w(\mathbf{x}) = 1 & \mathbf{x} \in S_{\text{Hex}} \\ w(\mathbf{x}) = 0 & \mathbf{x} \notin S_{\text{Hex}} \end{cases}$$

The fractional contribution of intra-trimer correlations is calculated as the ratio of $A_{0,\text{Intra}}(u)/(A_{0,\text{Intra}}(u) + A_{0,\text{Inter}}(u))$, where $A_{0,\text{Intra}}(u)$ and $A_{0,\text{Inter}}(u)$ are circularly averaged autocorrelation functions of Eqs. (2) and (3).

Inner helices 5, 6, and 7 see mostly other helices in the same trimer in the correlation at 30.5 Å, whereas outer helices, 1, 2, 3, and 4 have positive correlations in part with helices in the same trimer but also with those in the neighboring trimers. The fractional contribution of intra-trimer correlations is plotted in Fig. 4E, which

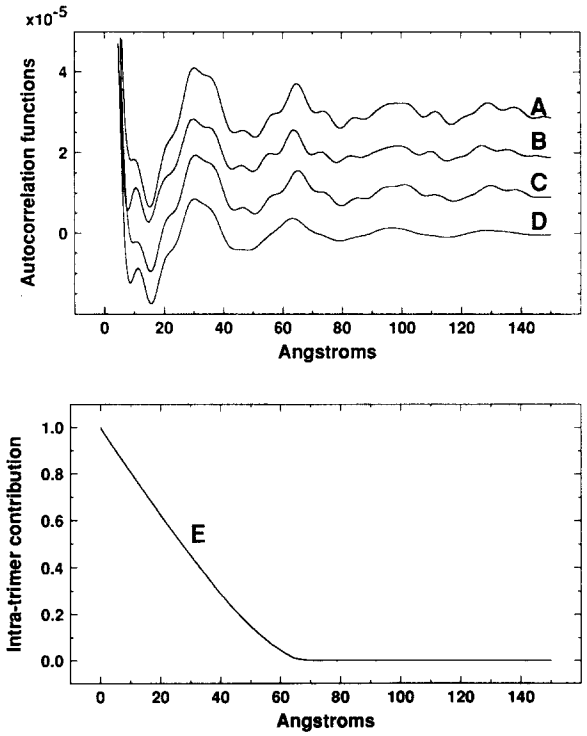

Fig. 4. Comparison of radial autocorrelation functions for the purple and blue membranes before and after dehydration, calculated from data in Fig. 1. (A) Purple membrane before dehydration; (B) purple membrane after dehydration; (C) blue membrane before dehydration; (D) blue membrane after dehydration; (E) fractional contribution of the intra-trimer correlations to the radial autocorrelation functions, $A_{0,\text{Intra}}(u)/(A_{0,\text{Intra}}(u) + A_{0,\text{Inter}}(u))$ (see Eqs. (2) and (3) for definition).

* Actual unit cell dimensions, as determined from the diffraction peak locations, were 63.1 and 62.1 Å for hydrated and dehydrated purple membranes and 63.4 Å for hydrated blue membranes. The consistently higher values obtained from the autocorrelation peak locations are most likely due to the breadth and slight asymmetry of the diffraction peaks. The autocorrelation peak locations were used because it was not possible to determine a reliable unit cell dimension from the very broad diffraction peaks of the dehydrated blue membranes.

shows that the peak at 30.5 Å is a combination of intra-trimer (44%) and inter-trimer correlations (56%) as opposed to 100% inter-trimer contribution in the case of 65 Å peak.

While the lattice dimension decreases appreciably during dehydration, it is apparent that the trimers mostly maintain their structure during the dehydration. Therefore the decrease in unit cell dimension should be attributed mainly to changes in the lipid region, between trimers. The contraction is about 200 $Å^2$ per unit cell, corresponding to areas of 3 to 4 lipids (the area of a lipid in PM is 60 $Å^2$ [34]). The lipid regions between trimers are about 5 to 10 Å wide (each lipid molecule can be modeled by an oval of 5 Å by 10 Å). Thus, the shrinkage of the lattice spacing introduces significant constraint on the arrangement of lipids. Note, however, that the 110 $Å^2$ contraction of the purple form, corresponding to the area of about 2 lipid molecules, does not produce lattice disorder. Therefore, an additional effect must be postulated to explain the larger shrinkage and disordering of the blue membrane lattice upon dehydration.

The crucial difference between purple and blue membrane preparations is presumably the absence of cations in the blue form. Low surface pH of the blue membranes, which is induced by the replacement of cations by protons, protonates carboxyl groups accessible to water [35] and breaks salt bridges near the membrane surfaces [15,16,23]. This leaves charged groups near the surface and they may generate long-range electrostatic interactions between proteins. Broken salt bridges not shielded by water could lead to strong coexistence of repulsive and attractive forces which could give rise to a translational/rotational disorder. The rotation of trimers would move surrounding lipids until they find new stable positions. This rearrangement of the lipids is coupled with the lateral shrinkage of the lipid regions and should lead to relative displacements of the trimers, generating a translational disorder of the lattice, thus resulting in broadening of the 2D Bragg peaks. It should be noted that a rotational disorder without displacement of trimers would not cause any broadening of the Bragg peaks; it would only change the X-ray diffraction intensities.

In a separate study, we found that anomalous X-ray profile diffraction from Tb^{3+} bound to PM shows two binding regions for cations in the vicinity of membrane surfaces at the height of lipid head groups on both sides which are 42 Å apart (S. Wakatsuki, K.O. Hodgson and S. Doniach, unpublished data, and [28]). The cations may therefore stabilize the purple form of the membranes by shielding long-range multipolar forces. On removal of the cations, carboxyl and lipid phosphate groups on the surfaces are unable to maintain salt bridges between lipids and proteins, which weakens the lattice. Removal of water will cause protonation of charged lipid groups and allow a rearrangement of the lipids with closer lateral packing. Zaccai et al. have shown that hydration occurs mainly in the lipid region [36,37]. Thus the lateral shrinkage of the lipid area would lead to the rotational and translational disorder of the protein trimers in the lattice as a result of their long-range competing attractive and repulsive interactions. This suggests that cations located in the vicinity of membrane surfaces stabilize the long-range periodicity of the trimer lattice. Removal of bound cations introduces long-range electrostatic interactions which are partially screened by water in the hydrated from. Dehydration can give rise to competing long-range attractive and repulsive forces which lead to the possibility of a disordered state.

These results clearly show that hydration is indispensable for maintaining the 2D crystal structure of deionized PM, while the presence of cations can sustain the lattice structure even upon dehydration. The demonstrated effects of dehydration with and without cations on screening of protein–protein, protein–lipid, or lipid–lipid interactions of blue membranes should be considered in crystallographic studies of other 2D protein-lipid membranes.

4. Acknowledgements

This research was supported by NIH Grant RR 1209 and data were recorded at both SSRL and NSLS which are supported by the DOE's Office of Basic Energy Science. S.W. was in part supported by The Murata Overseas Studies Foundation. Y.K. was supported by NIH program project grant GM27057. D.E. is supported by NSF Graduate Student Fellowship. We thank M. Rice for her assistance in development of the SAXS camera and in the experimental measurements. We are grateful to G. Ice, P. Zschack, and M. Engbretson for experimental assistance during the data collection on beamline X14A at NSLS.

5. References

[1] Stoeckenius, W., Lozier, R.H. and Bogomolni, R.A. (1979) Biochim. Biophys. Acta 505, 215–278.
[2] Unwin, P.N.T. and Henderson, R. (1975) J. Mol. Biol. 94, 425–440.
[3] Mitra, A.K. and Stroud, R.M. (1990) Biophys. J. 57, 301–312.
[4] Henderson, R., Baldwin, J.M., Downing, K.H., Lepault, J. and Zemlin, F. (1990) J. Mol. Biol. 213, 889–929.
[5] Blaurock, A. and Stoeckenius, W. (1971) Nature New Biol. 233, 152–155.
[6] Henderson, R. (1975) J. Mol. Biol. 93, 123–138.
[7] Koch, M.H., Dencher N.A., Oesterhelt, D., Plöhn, H.J., Rapp, G. and Büldt, G. (1991) EMBO J. 10, 521–526.
[8] Heyn, M.P., Westerhausen, J., Wallat, I. and Seiff, F. (1988) Proc. Natl. Acad. Sci. USA 85, 2146–2150.

[9] Popot, J.-L., Engelman, D.M., Gurel, O. and Zaccai, G. (1989) J. Mol. Biol. 210, 829–847.
[10] Papadopoulos, G., Dencher, N.A., Zaccai, G. and Buldt, G. (1990) J. Mol. Biol. 214, 15–19.
[11] Oesterhelt, D. and Stoeckenius, W. (1971) Nature New Biol. 233, 149.
[12] Drachev, L.A., Kaulen, A.D. and Skulachev, V.P. (1978) FEBS Lett. 87, 161–167.
[13] Mowery, P.C., Lozier, R.H., Chae, Q., Tseng, C.Y.-W., Taylor, M. and Stoeckenius, W. (1979) Biochemistry 18, 4100–4107.
[14] Kimura, Y., Ikegami, A. and Stoeckenius, W. (1984) Photochem. Photobiol. 40, 641–646.
[15] Szundi, I. and Stoeckenius, W. (1988) Biophys. J. 54, 227–232.
[16] Szundi, I. and Stoeckenius, W. (1989) Biophys. J. 56, 369–383.
[17] DeGroot, H.J.M., Smith, S.O., Courtin, J., VanDenBerg, E., Griffin, R.G., Lugtenburg, J. and Herzfeld, J. (1990) Biochemistry 29, 6873–6883.
[18] Subramaniam, S., Marti, T. and Khorana, H.G. (1990) Proc. Natl. Acad. Sci. USA 87, 1013–1017.
[19] Jang, D.-J., El-Sayed, M.A., Stern, L.J., Mogi, T. and Khorana, H.G. (1990) Proc. Natl. Acad. Sci. USA 87, 4103–4107.
[20] Metz, M., Siebert, F. and Engelhard, M. (1992) FEBS Lett. 303, 237–241.
[21] Fischer, U. and Oesterhelt, D. (1979) Biophys. J. 28, 211–230.
[22] Turner, G.J., Miercke, L.J.W., Thorgeirsson, T.E., Klinger, D.S., Betlach, M.C. and Stroud, R.M. (1993) Biochemistry 32, 1332–1337.
[23] Heyn, M.P., Dudda, C., Otto, H., Seiff, F. and Wallat, I. (1989) Biochemistry 28, 9166–9172.
[24] Seiff, F., Wallat, I., Ermann, P. and Heyn, M.P. (1985) Proc. Natl. Acad. Sci. USA 82, 3227–3231.
[25] Oesterhelt, D. and Stoeckenius, W. (1974) Methods Enzymol. 31, 667–678.
[26] Hendrix, J., Bordas, J., Gabriel, A. and Boulin, C. (1982) EMBL Annu. Res. Rep. 153.
[27] Hubbard, S.R. (1987) Small-angle X-ray Scattering Studies of Calcium-Binding Proteins. Ph.D. Thesis, Stanford University.
[28] Wakatsuki, S. (1990) Structural Studies of Bacteriorhodopsin using Synchrotron Small-angle X-ray Diffraction. Ph.D. Thesis, Stanford University.
[29] Rice, M. and Wakatsuki, S. (1991) A user's manual to the small-angle X-ray scattering/diffraction data acquisition system at SSRL. SSRL report, 09/91-R01.
[30] Wakatsuki, S., Eliezer, D., Gillis, N., Rice, M., Doniach, S. and Hodgson, K.O. (1992). Rev. Sci. Instrum. 63, 1736–1740.
[31] Habenschuss, A., Ice, G.E., Sparks, C.J. and Neiser, R.A. (1988) Nucl. Instr. Methods A266, 215–219.
[32] Hiraki, K., Hamanaka, T., Mitsui, T. and Kito, Y. (1981) Biochim. Biophys. Acta 647, 18–28.
[33] Kataoka, M. and Ueki, T. (1980) Acta Cryst. A36, 282–287.
[34] Glaeser, R.M., Jub, J.S. and Henderson, R. (1985) Biophys. J. 48, 775–780.
[35] Gerwert, K., Ganter, U.M., Siebert, F. and Hess, B. (1987) FEBS Lett. 213, 39–44.
[36] Rogan, P.K. and Zaccai, G. (1981) J. Mol. Biol. 145, 281–284.
[37] Zaccai, G. and Gilmore, D. (1979) J. Mol. Biol. 132, 181–191.